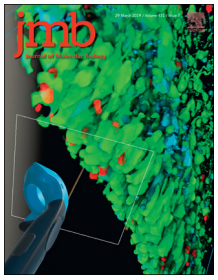

Structural Conservation of the Two Phosphoinositide-Binding Sites in WIPI Proteins

Ruobing Liang[1,3,†], **Jinqi Ren**[1,†], **Yong Zhang**[2] **and Wei Feng**[1,3]

*1 - **National Laboratory of Biomacromolecules,** CAS Center for Excellence in Biomacromolecules, Institute of Biophysics, Chinese Academy of Sciences, 15 Datun Road, Beijing 100101, China*
*2 - **Key Laboratory of RNA Biology,** CAS Center for Excellence in Biomacromolecules, Institute of Biophysics, Chinese Academy of Sciences, 15 Datun Road, Beijing 100101, China*
*3 - **College of Life Sciences,** University of Chinese Academy of Sciences, Beijing 100049, China*

***Correspondence to Wei Feng:** National Laboratory of Biomacromolecules, CAS Center for Excellence in Biomacromolecules, Institute of Biophysics, Chinese Academy of Sciences, 15 Datun Road, Beijing 100101, China.*
wfeng@ibp.ac.cn
https://doi.org/10.1016/j.jmb.2019.02.019
Edited by James H Hurley

Abstract

WIPI proteins are mammalian PROPPIN family members that bind to phosphoinositides and play prominent roles in autophagosome biogenesis. Two phosphoinositide-binding sites were previously described in yeast PROPPIN Hsv2 but remain to be determined in mammalian WIPI proteins. Here, we characterized four human WIPI proteins (WIPI1–4) and solved the structure of WIPI3. WIPI proteins can bind to PI(3)P and PI(3,5)P_2 and adopt a conventional seven-bladed β-propeller fold. The structure of WIPI3 revealed that WIPI proteins also contain two sites embedded in blades 5 and 6 for recognizing phosphoinositides, resembling that in Hsv2. Structural comparison further demonstrated that the two conserved phosphoinositide-binding sites in PROPPIN proteins are not identical but intrinsically tend to recognize different types of phosphoinositides. This work provides the structural evidence to support the conservation of the two phosphoinositide-binding sites in WIPI proteins and also uncovers the potential phosphoinositide-binding selectivity for each site.

Introduction

Autophagy is a highly conserved self-digestive process in eukaryotes that is essential for cellular nutrient homeostasis, protein quality control, and pathogen defense [1,2]. Macroautophagy (referred to as autophagy hereafter) is featured with a double-membrane structure termed autophagosome that sequesters and delivers aggregated proteins as well as damaged organelles to lysosome for degradation [3]. The degradation products through the autophagic process can be recycled back into the cellular synthesis pathways for reuse. Given the prominent role of autophagy in cellular homeostasis, dysfunction of this biological process is intimately related to a variety of disorders such as cancer, neurodegenerative disease, and aging [4–7].

Initiation of autophagy strictly depends on the synthesis of phosphatidylinositol 3-phosphate (PI(3)P) at specific membrane contact sites under various autophagic conditions [8]. This initial phosphoinositide signal can be sensed and decoded by the PI(3)P effectors that can recognize PI(3)P and recruit other proteins or protein complexes for the progression of autophagy. PROPPIN (β-propellers that bind phosphoinositides) proteins are the PI(3)P effectors that play prominent roles in autophagosome biogenesis [9]. In addition to binding to PI(3)P, PROPPIN proteins can interact with a variety of target proteins and likely function as a central hub to integrate the PI(3)P signal with other signaling pathways for controlling autophagy [10–14]. In yeast, there are three PROPPIN proteins, that is, Atg18, Atg21, and Hsv2. Structural studies of Hsv2 demonstrated that PROPPIN proteins are characterized by a seven-bladed β-propeller fold (blades 1 to 7) with a non-velcro closure topology [15,16]. Two sites (in blades 5 and 6) are located on the rim of the β-propeller, together with the hydrophobic

loop in blade 6, to contribute to the phosphoinositide-binding capacity of Hsv2 [15,16]. However, it remains to be determined whether the two phosphoinositide-binding sites previously described in yeast PROPPIN Hsv2 are structurally conserved in other PROPPIN proteins.

In mammals, there are four PROPPIN proteins, also termed WIPI (WD-repeat protein interacting with phosphoinositides) proteins (WIPI1 to WIPI4) [17]. WIPI1 and WIPI2 (the mammalian Atg18 orthologues) function upstream of the autophagic marker LC3 [18], that is, WIPI2b directly binds to ATG16L1, which is responsible for the efficient recruitment of the ATG12–ATG5–ATG16L1 complex and the lipidation of LC3 [11]; WIPI1 is likely to further facilitate WIPI2 during this process [19] and is also regarded as a molecular marker to monitor the process of autophagy [20]. On the other hand, WIPI4 can form a complex with ATG2A that may act as a tethering factor at the late stage of autophagosome completion [10,19,21]. Mutations of WIPI proteins are closely linked with cancer or age-related diseases [22], for example, mutations of WIPI4 cause beta-propeller protein-associated neurodegeneration (BPAN), a rare subtype of neurodegeneration with brain iron accumulation (NBIA) [23–25]; and mutations of WIPI3 lead to autosomal intellectual disability [26,27]. Emerging evidence demonstrated that WIPI proteins are likely to play more divergent roles in the different stages of autophagosome biogenesis [10,11,13,19]. However, the mechanism underlying the phosphoinositide recognition by WIPI proteins is not well understood.

In this study, we characterized four human WIPI proteins and determined the structure of WIPI3. WIPI proteins can bind to PI(3)P and PI(3,5)P_2. The structure of WIPI3 revealed that WIPI proteins adopt a conventional seven-bladed β-propeller fold and also contain two phosphoinositide-binding sites in blades 5 and 6, resembling that in yeast PROPPIN Hsv2. Structural comparison demonstrated that the two phosphoinositide-binding sites in PROPPIN proteins are not identical but intrinsic to recognize different types of phosphoinositides, supported by the simulation and mutational studies. Thus, the two phosphoinositide-binding sites are structurally conserved in WIPI proteins and the work also uncovers the potential phosphoinositide-binding selectivities of these two conserved sites.

Results and Discussion

Phosphoinositide-binding capacities of WIPI proteins

As the members of PROPPIN proteins in mammals, WIPI proteins contain the signature "L/FRRG" motif between blades 5 and 6 that was proposed to be dedicated for recognizing phosphoinositides [9] (Fig. S1). To examine the phosphoinositide-binding capacities of WIPI proteins, we performed the lipid strip-based binding assay for four human WIPI proteins (Fig. S2). In this assay, the full-length GFP-tagged WIPI proteins were expressed and purified by using the baculovirus expression system and were detected by the anti-GFP antibody on the lipid strip that carries different types of phospholipids. As expected, all the WIPI proteins (WIPI1 to WIPI4) can specifically recognize PI(3)P and PI(3,5)P_2 (Fig. S2), consistent with the previous biochemical characterization of WIPI proteins and other PROPPIN proteins in eukaryotes [19]. Notably, WIPI2 is capable of binding to PI(4)P and P(5)P (Fig. S2), also consistent with the previous studies of WIPI2 [28]. The similar phosphoinositide-binding capacities of WIPI proteins to other PROPPIN proteins are consistent with the high conservation of the "L/FRRG" motif in WIPI proteins and may also suggest a similar mechanism for recognition of phosphoinositides by them (Fig. S1 and see below for details).

Crystallization of human WIPI3

To investigate the mechanism for the phosphoinositide recognition by WIPI proteins, we set out to crystallize four human WIPI proteins and attempted to determine their structures by x-ray crystallography. In previous studies, much effort has been made on the structural characterization of PROPPIN proteins from different species [15,16,29]. Unfortunately, only the structures of two yeast PROPPIN proteins Hsv2 and Atg18 were determined, likely because most of PROPPIN proteins are the subunits of large protein complexes and tend to aggregate when expressed individually [15]. Consistent with these studies, all the four full-length WIPI proteins failed to be crystallized for structural determination during initial crystal screening. Among four WIPI proteins, the protein sample quality of WIPI3 is much better than the other three, but it also tends to easily aggregate at a high concentration. We then resorted to making the deletions of several flexible hydrophobic loops that are predicted to protrude from the β-propeller structural core (and could cause non-specific aggregation). As expected, the deletions of two loops (loop I: 75–80 and loop II: 264–281, Fig. 1a) could markedly enhance the protein sample quality of WIPI3 and the WIPI3-Δloop mutant is stable at a high concentration. On the other hand, WIPI3 is enriched with the cysteine residues that may need the sufficient amount of reductants to prevent the potential cysteine-mediated aggregation (Fig. S1). With the deletions of two loops and the addition of ~50 mM DTT as additive, the diffraction-quality crystals of WIPI3 were obtained for structural determination. In addition, the N-terminal seven

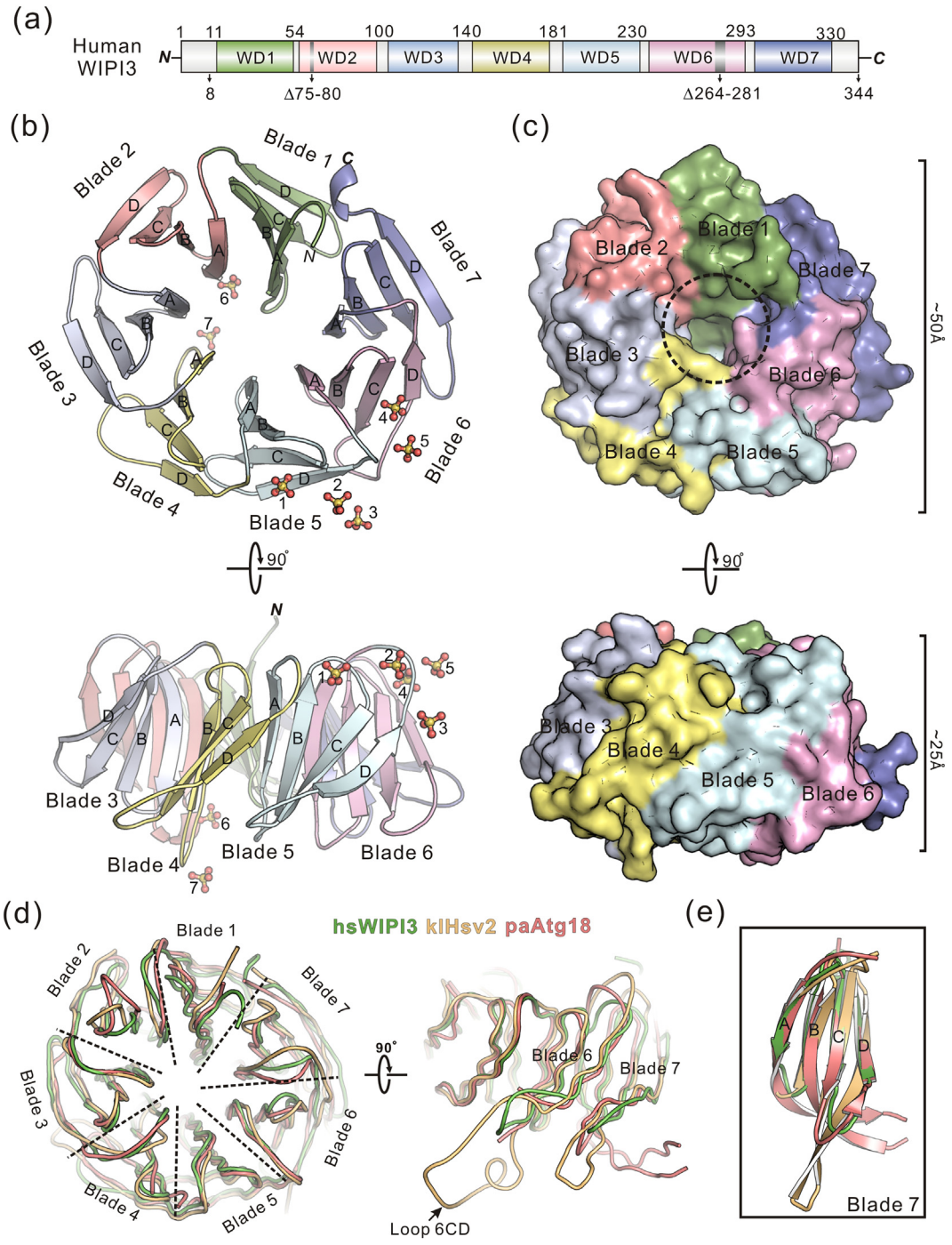

Fig. 1. Overall structure of the WIPI3-Δloop mutant. (a) Domain organization of human WIPI3. WIPI3 is composed of seven WD-repeats (WD1–7). The boundary of the WIPI3 construct used for crystallization is indicated. (b) Ribbon diagram of the WIPI3-Δloop mutant structure. Blades 1–7 are colored as the seven WD-repeats in panel a, and the seven sulfate ions (1–7) that bind to WIPI3 are shown as sticks. (c) Surface representation of the WIPI3-Δloop mutant structure. Blades 1–7 are colored as the seven WD-repeats in panel a. (d) Structure superimposition of the structures of *Homo sapiens* WIPI3 (hsWIPI3, colored in green), *Kluyveromyces lactis* Hsv2 (klHSV2, colored in wheat, PDB code: 4EXV), and *Pichia angusta* Atg18 (PaAtg18, colored in slate, PDB code: 5LTD). The C–D loop of blade 6 (loop 6CD) is indicated. (e) Structural comparison of blade 7 from hsWIPI3, klHsv2 and paAtg18. There are some obvious structural differences in blade 7 among these structures.

flexible residues was also removed and the final fragment boundary of WIPI3 for crystallization is from 8 to 344 (Fig. 1a).

Overall structure of the WIPI3-Δloop mutant

The structure of the WIPI3-Δloop mutant (with the deletions of two loops) was determined by the single-wavelength anomalous dispersion method and refined to 1.8 Å (Fig. 1b and Table 1). One molecule was found in the asymmetric unit of the crystal. Except for the extreme C-terminal tail, the overall structure of the WIPI3-Δloop mutant was well defined and the structure comprises the residues from 8 to 339 without two deleted loops (Fig. 1a–b). Moreover, some extra electron density maps with a tetrahedral shape were found in the refined structure. Since the crystals grew in a condition with a high concentration of sulfate (~1.6–2.0 M), these extra densities could be reasonably modeled with sulfate ions based on shape and size (Fig. S3a–b and see below for details).

Table 1. Data collection and structural refinement statistics

	Se-Met WIPI3	Native WIPI3
A. Diffraction data		
Space group	*C*2221	*C*2221
Wavelength (Å)	0.9785	0.9785
Cell dimensions		
a, *b*, *c* (Å)	47.2, 103.1, 127.0	46.36, 104.9, 124.9
α, *β*, *γ* (°)	90, 90, 90	90, 90, 90
Resolution (Å)	50–2.20 (2.28–2.20)[a]	50–1.80 (1.84–1.80)
Observed reflections	30,507 (2954)	28,765 (1811)
Unique reflections	5547 (656)	4425 (670)
R_{merge}[b] (%)	8.7 (39.4)	6.5 (23.0)
$I/\sigma(I)$	17.1 (4.2)	10.2 (3.0)
Multiplicity	5.5 (4.5)	6.5 (2.7)
Completeness (%)	99.5 (96.1)	99.6 (99.6)
B. Refinement		
R_{work}[c] (%)		16.5 (23.3)
R_{free}[d] (%)		20.4 (28.9)
Mean *B* factors (Å^2)		23.6
R.m.s. deviation[e]		
Bond length (Å)		0.010
Bond angles (°)		1.061
Ramachandran plot (%)		
Favored region		97.7
Allowed region		2.3
Disallowed region		0.0

[a] The values in parentheses refer to the highest-resolution shell.

[b] $R_{merge} = \sum_h \sum_i | I_i(h) - < I(h) > | / \sum_h \sum_i I_i(h)$, where I is the observed intensity and $< I >$ is the average intensity of multiple observations of symmetry-related reflection h.

[c] R_{work} is the R_{factor} for the working data set. $R_{factor} = \sum || F_o | - | F_c || / \sum | F_o |$, where $| F_o |$ and $| F_c |$ are observed and calculated structure factor amplitudes, respectively.

[d] R_{free} is the cross-validation R_{factor} computed for a randomly chosen subset of 5% of the total number of reflections, which were not used during refinement.

[e] Root mean square deviation from ideal values.

In the structure, the WIPI3-Δloop mutant adopts a seven-bladed β-propeller fold (blades 1 to 7) with a non-velcro closure topology similar to the yeast homologs Hsv2 and Atg18 (Fig. 1b–c). Each blade consists of four anti-parallel β-strands (from A to D), and the overall structure resembles a "disk" with the diameter of ~50 Å and thickness of ~25 Å (Fig. 1b–c). In addition, the C-terminal tail forms a short helix and packs into a pocket between blades 1 and 7 to further stabilize the overall structure (Fig. 1b). Based on the structure of the WIPI3-Δloop mutant, the two deleted loops (the B–C loop in blade 2 and the C–D loop in blade 6) should protrude from the β-propeller packing core and would not impact on the overall structure of WIPI3 (Fig. 1a–b), and therefore, the structure of the WIPI3-Δloop mutant can be used to represent that of WIPI3.

Consistent with the sequence similarity between WIPI3, Atg18 and Hsv2 (Fig. S1), the structure of WIPI3 can be well aligned with that of Hsv2 (PDB code: 4EXV) and Atg18 (PDB code: 5LTD) with RMSDs of ~1.39 and ~1.36 Å, respectively, for the backbone atoms (Fig. 1d). Although the three PROPPIN proteins WIPI3, Atg18, and Hsv2 show a conserved β-propeller fold, the prominent structural differences between them were found in blade 7 (Fig. 1d). In comparison to WIPI3, Hsv2 contains the extended β-strands C and D, while Atg18 possesses the extended β-strands A and B (Fig. 1e). Interestingly, the protruded β-strands A and B in Atg18 also consist of a number of hydrophobic residues (Figs. 1e and S1), although the potential function of this extended region remains to be determined. In the structural comparison, the additional difference between the three structures exists in the C–D loop of blade 6 (loop 6CD in Fig. 1d), which is likely to be caused by the deletion of this flexible loop in WIPI3 for structural determination (while this flexible loop is untraceable in the structure of Atg18) (Fig. 1d). Taken together, all the three PROPPIN proteins share a similar β-propeller structural fold with some variations in the loop regions that may contribute to the functional divergence of them.

Two conserved phosphoinositide-binding sites in WIPI proteins

With the structure of WIPI3, we attempted to further crystallize WIPI3 in complex with different phosphoinositides. However, all the trials failed because the crystals of WIPI3 grew well only in the condition with a high concentration of sulfate (that would block the interactions with phosphoinositides). We then had to resort to the sulfate-binding sites in the structure of WIPI3. Similar phenomena happened in the previous structural studies of Hsv2 (crystallized also with a high concentration of sulfate), which demonstrated that the sulfate-binding sites in the structure of Hsv2 are the

phosphoinositide-binding sites [15,16]. In the structure of Hsv2, two sulfate-binding sites (around the conserved "L/FRRG" motif) are located in blades 5 and 6, respectively (Fig. S4). Moreover, two similar phosphate-binding sites in blades 5 and 6 were also found in the structure of Atg18 (crystallized with phosphates) [29] (Fig. S4), supporting that the phosphoinositide-binding sites in PROPPIN proteins (that are positively charged) likely tend to bind to negatively charged sulfate/phosphate ions that would stabilize the proteins and facilitate crystallization.

Unexpectedly, there are three sulfate-binding sites (sites I to III) in the structure of WIPI3, and these three sites are all positively charged (Figs. 1b and S3c). Similar to Hsv2 and Atg18, the first two neighboring sites (sites I and II) are also located in blades 5 and 6 sandwiching the "L/FRRG" motif, while the third site (site III opposite to sites I and II) is located in the loop regions of blades 1 to 4 (Figs. 1b and S3). In site I of blade 5, there exist three sulfate ions that are recognized by the residues from blade 5 and the "L/FRRG" motif (Fig. 2a). Specifically, three sulfate ions together with a water molecule form an extensive electrostatic/hydrogen-bonding interaction network with H184, S204, K206, T208, and R211 from blade 5 and R225 from the "L/FRRG" motif

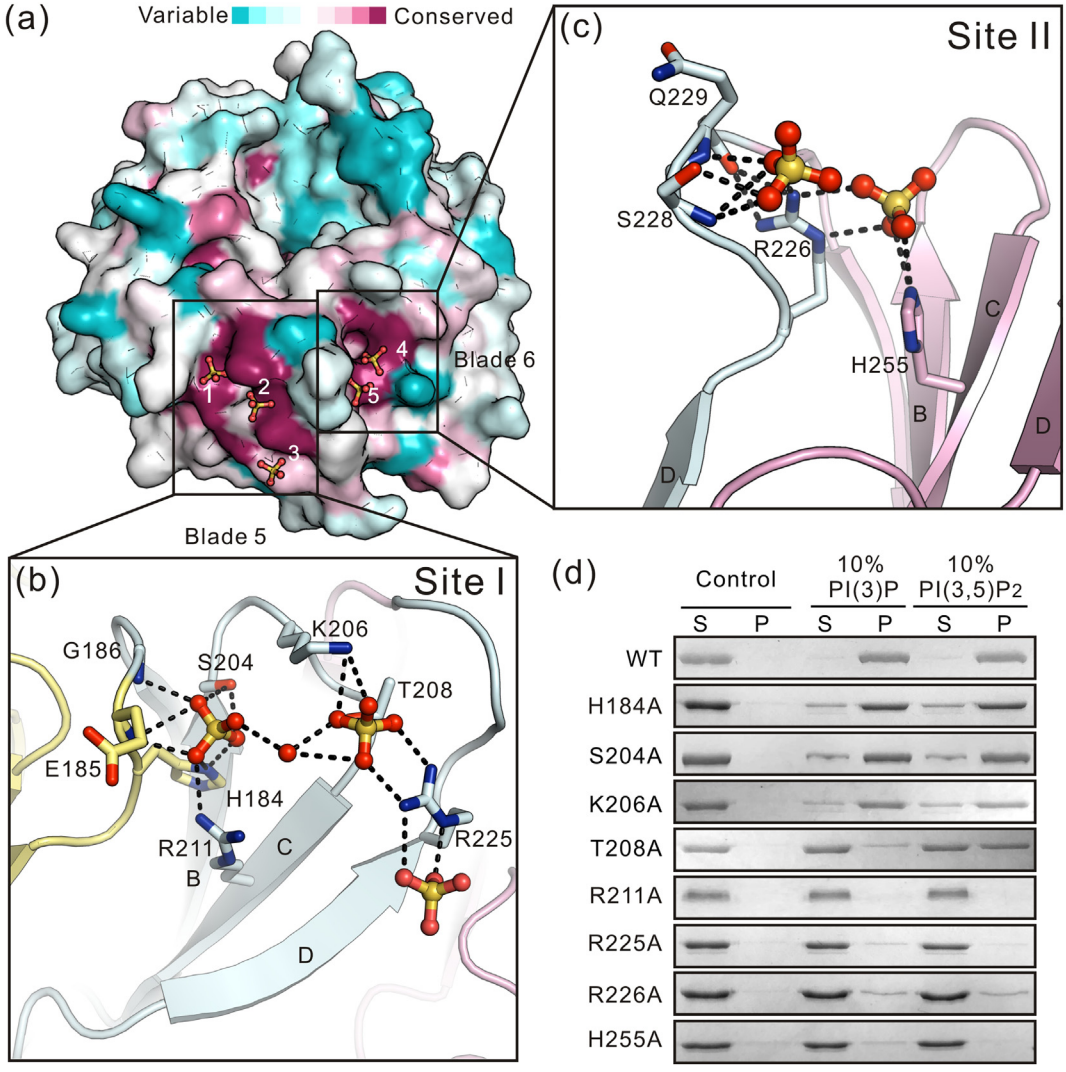

Fig. 2. Two conserved phosphoinositide-binding sites in WIPI3. (a) Surface representation of the WIPI3-Δloop mutant structure. The structure is colored according to the sequence conservation of human WIPI proteins. The two sulfate-binding sites are highlighted by black boxes, and the sulfate ions are shown as sticks. (b–c) Combined ribbon and stick representation of sulfate-binding site I (b) and sulfate-binding site II (c). The sulfate ions and the side chains of the residues involved in the binding interface are shown as sticks. Hydrogen bonds and salt bridges are indicated by dashed lines. (d) Liposome sedimentation assay of WIPI3 and its various mutants. The reconstituted multilamellar liposomes containing 10% PI(3)P or 10% PI(3,5)P_2 were used in this assay, and the reconstituted liposome without phosphoinositides was used as the negative control.

(Fig. 2b). In site II of blade 6, two sulfate ions are captured by the residues from the "L/FRRG" motif and blade 6 (Fig. 2a). Specifically, these two sulfate ions also form an electrostatic/hydrogen-bonding interaction network with R226 from the "L/FRRG" motif and S228 and H255 from blade 6 (Fig. 2c). On the other hand, in site III, two sulfate ions are recognized by the residues from blades 1 to 4 (Fig. S5). Specifically, two sulfate ions form the electrostatic/hydrogen-bonding interactions with N18 from blade 1, R62 from blade 2 and S151 from blade 4 (Fig. S5).

Based on the previous studies of PROPPIN proteins, the three sulfate-binding sites in WIPI3 described above are the potential phosphoinositide-binding sites. To investigate whether these sulfate-binding sites are involved in binding to phosphoinositides, we made mutations in these three sites and checked the lipid-binding capacities of the mutants by the liposome-sedimentation assay (with the reconstituted liposome containing either PI(3)P or PI(3,5)P_2) (Fig. 2d). In comparison to the wild-type full-length protein, mutations of the essential residues in site I (i.e., H184A, S204A, K206A, T208A, R211A, and R225A) that are responsible for binding to sulfate ions impaired (or abolished) the lipid-binding capacity of WIPI3 (Fig. 2d), indicating that this site is involved in phosphoinositide binding. Similar results were obtained for mutations of the essential residues in site II (i.e., R226A and H255A) (Fig. 2d). In contrast, mutations of the residues in site III (i.e., R62A) had little impact on the lipid-binding capacity of WIPI3 (Fig. S5), suggesting that this site is unlikely to participate in phosphoinositide binding. Thus, among the three sulfate-binding sites in the structure of WIPI3, the first two sites (sites I and II) in blades 5 and 6 are the primary phosphoinositide-binding sites but site III is not, which is consistent with the two sites previously found in other PROPPIN proteins [15,16] (Figs. 2a and S4). Supporting this conclusion, the essential residues in sites I and II (for sulfate-binding) are highly conserved in WIPI proteins, while the residues in site III are diverse (Figs. 2a and S5). On the other hand, the previous studies of PROPPIN proteins demonstrated that the interaction sites for their binding partners were largely narrowed down to the regions around site III [10,21]. Thus, it is possible that site III might be involved in the protein–protein interaction (rather than lipid binding), and it would be interesting to further investigate whether site III can mediate the binding to other proteins.

Two phosphoinositide-binding sites in PROPPIN proteins are not identical

In the two phosphoinositide-binding sites of Hsv2 and Atg18, only one sulfate/phosphate ion was clearly traced possibly due to the limited resolution of the two structures (Fig. S4). However, in the structure of WIPI3 at high resolution, much more sulfate ions were found in the two conserved phosphoinositide-binding sites, and the sulfate-binding capacities of these two sites are somewhat distinct; that is, site I in blade 5 binds to three sulfate ions, but site II in blade 6 only captures two (Fig. 2a), suggesting that the two sites in blades 5 and 6 are not identical and may possess certain selectivities for different phosphoinositides. To investigate the structural similarity and potential difference between the two phosphoinositide-binding sites in WIPI3, we compared the overall conformations of these two sites in detail (Fig. 3a). The two sites could be well aligned with each other (with the RMSD of ~0.61 Å for the backbone atoms) and contain a similar preformed pocket that is constructed by the residues from blades 5 and 6 (Fig. 3a). More specifically, the three residues H184, S204, and R211 from site I of blade 5 match the three residues R226, S249, and H255 from site II of blade 6 and form the conserved core of the two pockets for recognizing phosphoinositides (Fig. 3a and d). However, the peripheral residues of the two pockets are somewhat different; for example, R225 from site I of blade 5 is unlikely to be well corresponding to Q290 from site II of blade 6 (Fig. 3a and d). In addition, the position of T208 from site I of blade 5 is also different from that of T253 from site II of blade 6 due to the lack of one residue in blade 6 (Fig. 3a and d). Thus, the two phosphoinositide-binding sites from blades 5 and 6 in WIPI3 are not completely identical.

The structural differences between the two phosphoinositide-binding sites in WIPI3 prompted us to further investigate the phosphoinositide-binding sites in other PROPPIN proteins. We next compared the two phosphoinositide-binding sites in Hsv2 and Atg18 (Fig. 3b–c). Similar to WIPI3, the two sites from blades 5 and 6 in Hsv2 and Atg18 could be well aligned with each other (with RMSDs of ~0.70 and ~1.19 Å, respectively, for the backbone atoms) and contain a similar preformed phosphoinositide-binding pocket (Fig. 3b–c). Moreover, the three residues in the central core of the pocket from site I of blade 5 (H178, S198, and R205 in Hsv2; H221, S241, and R248 in Atg18) are well corresponding to the three residues in that from site II of blade 6 (R220, S243, and H249 in Hsv2; R263, S286, and H292 in Atg18) (Fig. 3b–d), supporting the conserved phosphoinositide-binding feature in PROPPIN proteins. In contrast, also similar to WIPI3, the peripheral residues of the two pockets in Hsv2 and Atg18 are somewhat different (D200 *versus* K245 in Hsv2; K243 *versus* T288 in Atg18) and the position of the residue threonine from site I of blade 5 (T202 in Hsv2; T245 in Atg18) is also different from that of the residue threonine from site II of blade 6 (T247 in Hsv2; T290 in Atg18) (Fig. 3b–d). Consistent with the structural comparison, the

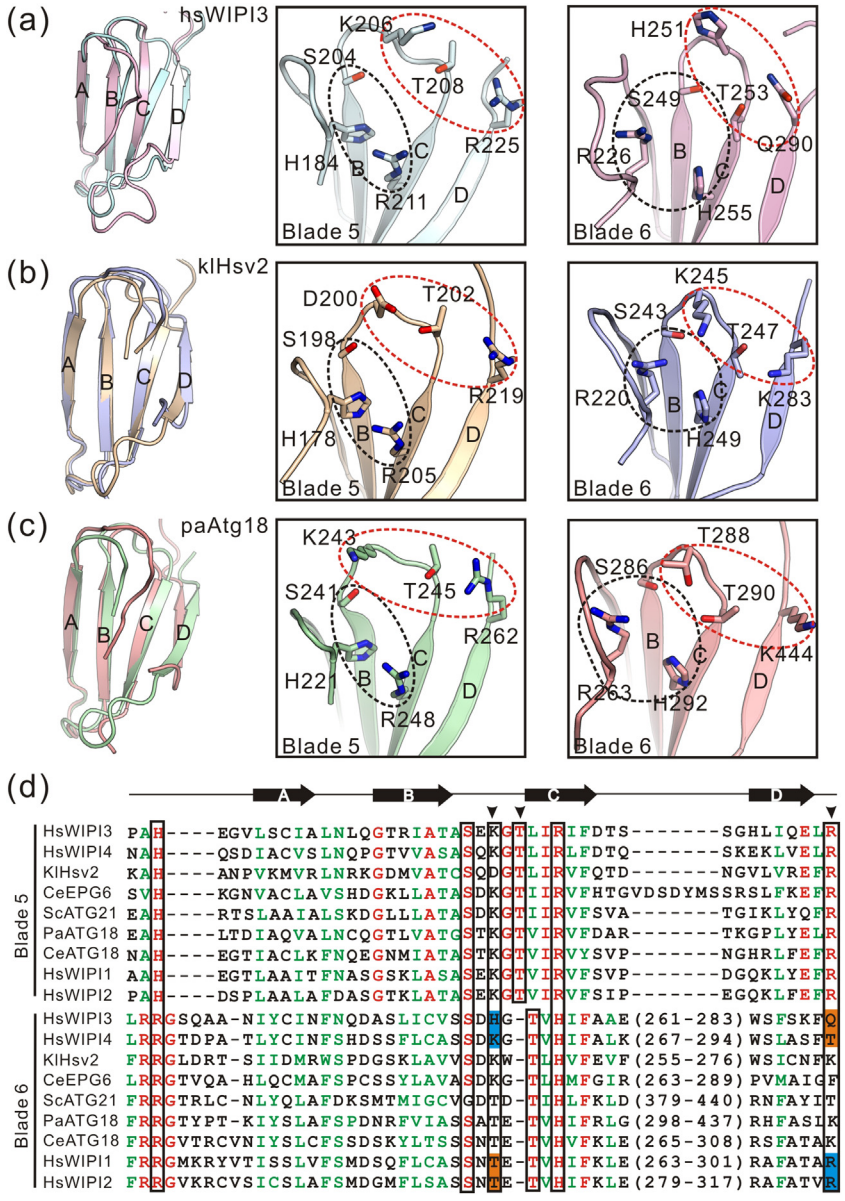

Fig. 3. Two putative phosphoinositide-binding sites in PROPPIN proteins are not identical. (a–c) Structural comparison of the two phosphoinositide-binding sites in blades 5 and 6 from hsWIPI3 (a), paAtg18 (b), and klHsv2 (c). The side chains of the residues involved in the sulfate/phosphate-binding interface are shown as sticks, and the sulfate/phosphate ions in the structures are removed for clarity. The conserved cores of the two pockets are highlighted by black circles, and the divergent peripheral residues of the two pockets are highlighted by red circles. (d) Structure-based sequence alignment of the phosphoinositide-binding blades 5 and 6 from different PROPPIN proteins. The identical residues are colored in red, and the highly conserved residues are colored in green. The key residues for recognition of phosphoinositides are indicated by black boxes. The divergent peripheral residues are indicated by arrowheads. The different peripheral residues in site II of WIPI1–4 are also highlighted.

sequence alignment also demonstrated that the residues that form the central core of the two pockets in blades 5 and 6 are highly conserved, but the peripheral residues of the two pockets are somewhat diverse (Fig. 3d). Taken together, based on all the above structural analyses of WIPI3, Hsv2, and Atg18, the peripheral structural differences between the two conserved phosphoinositide-binding sites are likely to be a common feature in PROPPIN proteins.

Potential phosphoinositide-binding selectivities of the two sites in WIPI proteins

Biochemical characterization of WIPI proteins demonstrated that they can recognize two types of phosphoinositides, that is, PI(3)P and PI(3,5)P_2 (Fig. S2). Based on the structural comparison of the two phosphoinositide-binding sites in WIPI3, two positively charged residues K206 and R225 are located at the periphery of site I of blade 5 (Fig. 3a), indicating that this site is likely to be capable of accommodating more negatively charged phosphate groups and would therefore tend to recognize PI(3,5)P_2. In contrast, the less positively charged site II of blade 6 would prefer to recognize PI(3)P (Fig. 3a). Consistent with this speculation, three sulfate ions bind to site I of blade 5, but only two interact with site II of blade 6 (Figs. 2a and S3).

To further check whether the two sites of WIPI3 possess certain selectivities for different phosphoinositides, we next performed the molecular dynamics

(MD) simulations of the two phosphoinositide-binding sites in complex with PI(3)P or PI(3,5)P_2 in solution (Fig. 4a–b). Based on the positions of bound sulfate ions in the structure of WIPI3 (Fig. 2b–c), we docked the negatively charged inositide head of PI(3)P or PI(3,5)P_2 into the two sites and then performed the MD simulations. As expected, in site I of blade 5, PI(3,5)P_2 stably binds to the pocket throughout the simulations, whereas PI(3)P leaves from the pocket at the late stage of the simulations possibly due to the relatively weak interactions between them (Fig. 4a), suggesting that this site is more likely to favor the more negatively charged PI(3,5)P_2. In contrast, in site II of blade 6, PI(3)P binds to the pocket constantly throughout the simulations, whereas PI(3,5)P_2 interacts with the pocket fluctuatingly during the simulations (Fig. 4b), indicating that this site tends to prefer the less negatively charged PI(3)P.

Based on the structural analysis and MD simulations (Figs. 3a and 4a–b), we made the point mutations in both sites I and II of WIPI3 (K206A and Q290R, respectively); that is, the K206A mutation in the peripheral region of site I would impair the binding of PI(3,5)P_2, while the Q290R mutation in the peripheral region of site II would enhance the binding of PI(3,5)P_2. We further checked the lipid-binding capacities of the two mutants by the liposome-sedimentation assay (Fig. 4c). Based on the previous studies of PROPPIN proteins [15], the reconstituted liposome we used was composed of the lower concentration (3%) of PI(3)P or PI(3,5)P_2. As expected, the K206A mutation in site I severely impaired the binding of WIPI3 to the PI(3,5)P_2-containing liposome, whereas the Q290R mutation in site II could enhance the binding of WIPI3 to the PI(3,5)P_2-containing liposome (Fig. 4c). On the other hand, in comparison to wild-type WIPI3, no obvious lipid-binding changes of the two mutants were observed for binding to the PI(3)P-containing liposome (Fig. 4c). Taken together, all these data demonstrated that the two phosphoinositide-binding

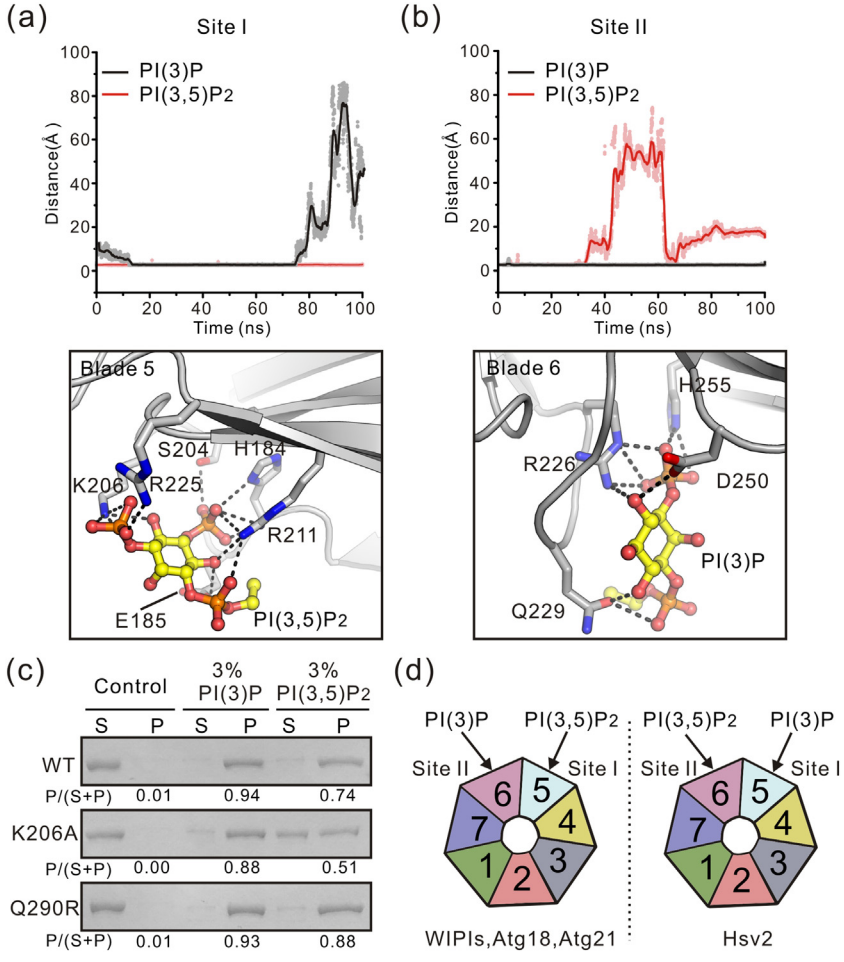

Fig. 4. Potential phosphoinositide-binding specificities of the two sites in WIPI3. (a) MD simulations of the WIPI3 structure, with the phosphoinositide-binding site I being occupied by PI(3)P or PI(3,5)P_2. The relative distances (between R225 and phosphoinositide) over the time course of the simulations are plotted in the upper panel. The final snapshot at 100 ns of the simulation for WIPI3 in complex with PI(3,5)P_2 is presented in the lower panel. The side chains of the residues involved in the interaction interface are shown as sticks, and hydrogen bonds and salt bridges are indicated by dashed lines. (b) MD simulations of the WIPI3 structure, with the phosphoinositide-binding site II being occupied by PI(3)P or PI(3,5)P_2. The relative distances (between R226 and phosphoinositide) over the time course of the simulations are plotted in the upper panel. The final snapshot at 100 ns of the simulation for WIPI3 in complex with PI(3)P is presented in the lower panel. (c) Liposome sedimentation assay of WIPI3 and its mutants with the lower concentration (3%) of PI(3)P or PI(3,5)P_2. The ratio of protein in pellet fraction (P) to total protein (supernatant fraction and pellet fraction, S + P) was estimated and labeled at the bottom for each protein. (d) A schematic working model for the potential phosphoinositide-binding selectivities of the two sites in PROPPIN proteins.

sites from blades 5 and 6 in WIPI3 contain certain intrinsic selectivities for different phosphoinositides; that is, site I of blade 5 prefers PI(3,5)P_2, while site II of blade 6 favors PI(3)P.

Recognition of different phosphoinositides by PROPPIN proteins

Previous structural studies of PROPPIN proteins focused on yeast homologs Hsv2 and Atg18 and demonstrated that they adopt a seven-bladed β-propeller fold and contain two phosphoinositide-binding sites [15,16]. However, due to the poor protein sample quality, mammalian homologs WIPI proteins were less structurally characterized. In this work, we characterized WIPI proteins and determined the structure of WIPI3 (with deletions of two flexible loops for improving the protein sample quality) (Fig. 1). The structure of WIPI3 revealed that WIPI proteins adopt a similar structural fold and also contain two sites located in blades 5 and 6 for recognizing phosphoinositides (Fig. 2), thus supporting the structural conservation of the two phosphoinositide-binding sites in PROPPIN proteins.

PROPPIN proteins were found to be capable of specifically recognizing different types of phosphoinositides such as PI(3)P and PI(3,5)P_2 [9] (Fig. S2). The structural comparison of the two phosphoinositide-binding sites in WIPI3 demonstrated that these two conserved sites are not completely identical and may contain the intrinsic tendency to recognize PI(3)P or PI(3,5)P_2 (Fig. 3), further supported by the MD simulations of each site in complex with different phosphoinositides and the mutational studies (Fig. 4a–c). Since the two phosphoinositide-binding sites in Hsv2 and Atg18 exhibit the similar structural differences at the peripheries (Fig. 3), the phosphoinositide-binding preference for each site may also extend to other PROPPIN proteins. In Hsv2, the negatively charged residue D200 is located at the periphery of site I of blade 5, but the same position of site II of blade 6 is occupied by K245 (Fig. 3), indicating that, in contrast to WIPI3, site I of blade 5 favors PI(3)P but site II of blade 6 prefers PI(3,5)P_2 (Fig. 4d). Consistent with this speculation, previous studies of Hsv2 demonstrated that disruptions of site I of blade 5 still retain the binding to PI(3,5)P_2 but not PI(3)P [15]. On the other hand, in Atg18, no negatively charged residues are located at the peripheries of the two sites that would exhibit the similar phosphoinositide-binding preferences to that of WIPI3 (Figs. 3 and 4d). Supporting this structural feature, Atg18 was found to strongly interact with PI(3,5)P_2 and disruptions of site I of blade 5 severely impaired the binding to PI(3,5)P_2 [29]. Taken together, in PROPPIN proteins, the structural differences at the peripheries of the two phosphoinositide-binding sites are likely to be able to fine tune the selectivities for different phosphoinositides.

The structure-based sequence alignment demonstrated that the peripheral residues of site I in WIPI1–4 are identical, but the residues of site II are somewhat different between WIPI1 and WIPI4 (Fig. 3d). More specifically, in site II, WIPI1 and WIPI2 contain the similar set of peripheral residues that are distinct from that in WIPI3 and WIPI4, that is, WIPI1–T253/WIPI2–T269 *versus* WIPI3–H251/WIPI4–K257, and WIPI1–R308/WIPI2–R324 *versus* WIPI3–Q290/WIPI4–T301 (Fig. 3d). Based on the structural analysis and MD simulations (Figs. 3 and 4), WIPI1–R308/WIPI2–R324 tends to be more important for recognizing the position 5 phosphate group of phosphoinositides, which might provide an explanation for WIPI2 to bind to a broader range of phosphoinositides (Fig. S2). Consistent with this, WIPI2 has been reported to bind to PI(5)P and can regulate a PI(3)P-independent autophagy process [28]. However, WIPI1 does not exhibit the similar capacity to WIPI2 and the functional importance of WIPI1 in autophagy process is not well understood at the current stage.

In summary, this work provides the structural evidence to support the conservation of the two phosphoinositide-binding sites in PROPPIN proteins (from yeast to mammals) and also reveals the potential phosphoinositide-binding selectivities for these conserved sites that are determined by the peripheral structural differences.

Materials and Methods

Protein expression and purification

The cDNA encoding human WIPI1–4 full-length proteins were generous gifts from Dr. Hong Zhang, Institute of Biophysics, CAS. The deletions of the two loops (75–80 and 264–281) and other point mutations in WIPI3 were performed by using the standard PCR-based mutagenesis method and confirmed by DNA sequencing. For expression of full-length WIPI3, the WIPI3-Δloop mutant, and other various mutants, the DNA sequences were each cloned into a modified pET32a vector. Recombinant proteins were expressed in *Escherichia coli* BL21 (DE3) host cells at 16 °C. The GB1-His_6-tagged fusion proteins were purified by Ni^{2+}-Sepharose 6 Fast Flow (GE Healthcare) affinity chromatography followed by size-exclusion chromatography (Superdex-200 26/60; GE Healthcare). After cleavage of the tag, the resulting proteins were further purified by another step of size-exclusion chromatography with buffer containing 50 mM Tris–HCl (pH 8.0), 100 mM NaCl, 1 mM EDTA, and 50 mM DTT. For expression of human WIPI1–4 full-length proteins, the DNA sequences were each cloned into a modified pFastBac1 vector. The GFP-tagged recombinant proteins were expressed in a baculovirus system in Sf9

(Invitrogen) insect cells and were purified by Ni^{2+}-Sepharose 6 Fast Flow (GE Healthcare) and Strep-Tactin (IBA) affinity chromatography followed by size-exclusion chromatography.

Crystallization

Crystals of the WIPI3-Δloop mutant were grown in 1.6–2.0 M ammonium sulfate and 0.1 M Tris–HCl (pH 7.0). All the crystals were obtained using the sitting drop vapor diffusion method at 16 °C. Before being flash-frozen in liquid nitrogen, crystals were soaked in the mother liquor supplemented with 20% (v/v) glycerol for cryo-protection.

Data collection and structural determination

All the diffraction data sets were collected at the beamline BL17U of the Shanghai Synchrotron Radiation Facility with a wavelength of 0.979 Å at 100K [30]. Data sets were integrated and scaled with HKL2000 [31]. The structure of the WIPI3-Δloop mutant was determined using the single-wavelength anomalous dispersion method with anomalous dispersion from the selenium atoms by the program AutoSol in PHENIX [32]. Additional missing residues were manually modeled into the structure according to the $2F_o - F_c$ and $F_o - F_c$ electron density maps. The structure was further fitted and rebuilt with COOT [33] and refined with PHENIX [32]. The protein structure figures were prepared with PyMOL (https://pymol.org/2/). The statistics for the data collection and structural refinement are summarized in Table 1.

Liposome sedimentation assay

The liposome sedimentation assay was performed with reconstituted multilamellar liposomes. The reconstituted liposomes were prepared as described previously [15]. Briefly, DOPS (1,2-dioleoyl-sn-glycero-3-phospho-L-serine) (Avanti, 840035), DOPC (1,2-dioleoyl-sn-glycero-3-phosphocholine) (Avanti, 850375), and POPE (1-palmitoyl-2-oleoyl-sn-glycero-3-phosphoethanolamine) (Avanti, 850757) were each dissolved in chloroform. PI(3)P (dipalmitoyl phosphatidylinositol 3-phosphate) (Echelon, P-3016) was dissolved in a mixture of methanol, chloroform, and water. PI(3,5)P_2 (dipalmitoyl phosphatidylinositol 3,5-bisphosphate) (Echelon, P-3516) was dissolved in a mixture of methanol and water. Lipids were then mixed at the appropriate ratios to preserve the same net charge on liposomes by varying the PS mole fraction. The charges were assumed to be as follows: PS, −1; PI(3)P, −3; and PI(3,5)P_2, −4. The final compositions in mole percent were as follows: the 3% PI(3)P-containing liposome [3% PI(3)P, 66% PS, 23.5% PC, 7.5% PE], the 10% PI(3)P-containing liposome [10% PI(3)P, 45% PS, 37.5% PC, 7.5% PE], the 3% PI(3,5)P_2-containing liposome [3% PI(3,5)P_2, 63% PS, 26.5% PC, 7.5% PE], the 10% PI(3,5)P_2-containing liposome [10% PI(3,5)P_2, 35% PS, 47.5% PC, 7.5% PE], and the control liposome (75% PS, 17.5% PC,7.5% PE). The lipid mixture was pipetted into glass tubes, and the organic solvent was evaporated with a stream of nitrogen. Residual solvent was removed by overnight incubation in vacuum. Lipids were resuspended in the buffer [40 mM Hepes (pH 7.4), 150 mM NaCl, 1 mM DTT, 1 mM EDTA] at 4 °C, and liposomes were prepared by vigorous vortex.

For the liposome sedimentation assay, the full-length WIPI3 and its various mutants (with point mutations) were used. Equal volumes of proteins and liposomes (25 μl) were mixed and incubated at 4 °C for 30 min. The final protein and lipid concentrations were 1.5 μM and 1 mg/ml, respectively. The protein/liposome mixture was sedimented by centrifugation at 16,000*g* for 20 min. The pellet and supernatant fractions were analyzed by SDS-PAGE with Coomassie blue staining.

MD simulations of WIPI3 in complex with phosphoinositides

Both PI(3)P and PI(3,5)P_2 were docked into the two phosphoinositide-binding sites of WIPI3 that bind to sulfate ions in the crystal structure using Autodock4.2 software package [34]. As expected, the binding conformations of the phosphate groups of PI(3)P and PI(3,5)P_2 with large score in the two sites fit well the positions of sulfate ions in the crystal structure. The four docked WIPI3 complexes (with each site binding to PI(3)P and PI(3,5)P_2, respectively) were then solvated in a $83 \times 81 \times 76$ $Å^3$ water box, and $42Na^+/39Cl^-$ were added to neutralize the system. The NAMD package [35] and CHARMM36 all-atom force field [36–38] were used for energy minimizations and MD simulations. Under periodic boundary condition, a 12-Å cutoff was used for van der Waals interactions, and Particle Mesh Ewald summation was used to calculate the electrostatic interactions. For each simulation, energy was first carefully minimized to avoid any possible clashes. The energy-minimized systems were then equilibrated in two steps, that is, 2-ns simulation with constraining the heavy atoms of the protein-PI(3)P/PI(3,5)P_2 complex and 4-ns simulation with constraining the backbone atoms of the protein-PI(3)P/PI(3,5)P_2 complex. With the equilibrated structures, ~100-ns free MD simulations were performed for each docked model. During the simulations, the temperature was controlled at 310K by Langevin dynamics, and the pressure was controlled at 1 atm by the Langevin piston method. SHAKE method was used on all hydrogen-containing bonds to allow a 2-fs time step. The trajectories were analyzed with VMD program [39].

Accession numbers

The atomic coordinate of the WIPI3-Δloop mutant has been deposited in the Protein Data Bank with the accession number 6IYY.

Acknowledgments

We thank the beam-line BL17U of the Shanghai Synchrotron Radiation Facility for the beam time. This work was supported by grants from the National Key R&D Program of China (2017YFA0503501) and the National Natural Science Foundation of China (31770786, 31600608, 31829001, and 31600622).

Appendix A. Supplementary data

Supplementary data to this article can be found online at https://doi.org/10.1016/j.jmb.2019.02.019.

Received 20 December 2018;
Received in revised form 14 February 2019;
Accepted 14 February 2019
Available online 22 February 2019

Keywords:
autophagy;
PROPPIN;
phosphoinositide;
WIPI;
x-ray crystallography

†R.L. and J.R. contributed equally to this work.

Abbreviations used:
WIPI, WD-repeat protein interacting with phosphoinositides; PROPPIN, β-propellers that bind phosphoinositides; PI(3)P, phosphatidylinositol 3-phosphate; PI(3,5)P_2, phosphatidylinositol 3,5-bisphosphate; Atg, autophagy-related protein; BPAN, beta-propeller protein-associated neurodegeneration.

References

[1] N. Mizushima, T. Yoshimori, Y. Ohsumi, The role of Atg proteins in autophagosome formation, Annu. Rev. Cell Dev. Biol. 27 (2011) 107–132.
[2] X. Wen, D.J. Klionsky, An overview of macroautophagy in yeast, J. Mol. Biol. 428 (2016) 1681–1699.
[3] C.A. Lamb, T. Yoshimori, S.A. Tooze, The autophagosome: origins unknown, biogenesis complex, Nat. Rev. Mol. Cell Biol. 14 (2013) 759–774.
[4] B. Levine, G. Kroemer, Autophagy in the pathogenesis of disease, Cell. 132 (2008) 27–42.
[5] V. Deretic, T. Saitoh, S. Akira, Autophagy in infection, inflammation and immunity, Nat. Rev. Immunol. 13 (2013) 722–737.
[6] E. Wong, A.M. Cuervo, Autophagy gone awry in neurodegenerative diseases, Nat. Neurosci. 13 (2010) 805–811.
[7] D.C. Rubinsztein, G. Marino, G. Kroemer, Autophagy and aging, Cell. 146 (2011) 682–695.
[8] E.L. Axe, S.A. Walker, M. Manifava, P. Chandra, H.L. Roderick, A. Habermann, et al., Autophagosome formation from membrane compartments enriched in phosphatidylinositol 3-phosphate and dynamically connected to the endoplasmic reticulum, J. Cell Biol. 182 (2008) 685–701.
[9] S.K. Dove, R.C. Piper, R.K. McEwen, J.W. Yu, M.C. King, D.C. Hughes, et al., Svp1p defines a family of phosphatidylinositol 3,5-bisphosphate effectors, EMBO J. 23 (2004) 1922–1933.
[10] J.X. Zheng, Y. Li, Y.H. Ding, J.J. Liu, M.J. Zhang, M.Q. Dong, et al., Architecture of the ATG2B–WDR45 complex and an aromatic Y/HF motif crucial for complex formation, Autophagy. 13 (2017) 1870–1883.
[11] C. Dooley Hannah, M. Razi, E.J. Polson Hannah, E. Girardin Stephen, I. Wilson Michael, Sharon A. Tooze, WIPI2 links LC3 conjugation with PI3P, autophagosome formation, and pathogen clearance by recruiting Atg12–5-16L1, Mol. Cell 55 (2014) 238.
[12] T. Kotani, H. Kirisako, M. Koizumi, Y. Ohsumi, H. Nakatogawa, The Atg2–Atg18 complex tethers pre-autophagosomal membranes to the endoplasmic reticulum for autophagosome formation, Proc. Natl. Acad. Sci. U. S. A. 115 (41) (2018) 10363–10368.
[13] T. Proikas-Cezanne, Z. Takacs, P. Donnes, O. Kohlbacher, WIPI proteins: essential PtdIns3P effectors at the nascent autophagosome, J. Cell Sci. 128 (2015) 207–217.
[14] Q. Lu, P.G. Yang, X.X. Huang, W.Q. Hu, B. Guo, F. Wu, et al., The WD40 repeat PtdIns(3)P-binding protein EPG-6 regulates progression of omegasomes to autophagosomes, Dev. Cell 21 (2011) 343–357.
[15] S. Baskaran, M.J. Ragusa, E. Boura, J.H. Hurley, Two-site recognition of phosphatidylinositol 3-phosphate by PROPPINs in autophagy, Mol. Cell 47 (2012) 339–348.
[16] R. Krick, R.A. Busse, A. Scacioc, M. Stephan, A. Janshoff, M. Thumm, et al., Structural and functional characterization of the two phosphoinositide binding sites of PROPPINs, a beta-propeller protein family, Proc. Natl. Acad. Sci. U. S. A. 109 (2012) E2042–E2049.
[17] T. Proikas-Cezanne, S. Waddell, A. Gaugel, T. Frickey, A. Lupas, A. Nordheim, WIPI-1alpha (WIPI49), a member of the novel 7-bladed WIPI protein family, is aberrantly expressed in human cancer and is linked to starvation-induced autophagy, Oncogene. 23 (2004) 9314–9325.
[18] E. Itakura, N. Mizushima, Characterization of autophagosome formation site by a hierarchical analysis of mammalian Atg proteins, Autophagy. 6 (2010) 764–776.
[19] D. Bakula, A.J. Müller, T. Zuleger, Z. Takacs, M. FranzWachtel, A. Thost, et al., WIPI3 and WIPI4 β-propellers are scaffolds for LKB1-AMPK-TSC signalling circuits in the control of autophagy, Nat. Commun. 8 (2017) 15637.
[20] T. Proikas-Cezanne, S. Ruckerbauer, Y.D. Stierhof, C. Berg, A. Nordheim, Human WIPI-1 puncta-formation: a novel assay to assess mammalian autophagy, FEBS Lett. 581 (2007) 3396–3404.
[21] S. Chowdhury, C. Otomo, A. Leitner, K. Ohashi, R. Aebersold, G.C. Lander, et al., Insights into autophagosome biogenesis from structural and biochemical analyses of the

ATG2A–WIPI4 complex, Proc. Natl. Acad. Sci. 115 (2018) E9792-E801.
[22] D. Bakula, Z. Takacs, T. Proikas-Cezanne, WIPI beta-propellers in autophagy-related diseases and longevity, Biochem. Soc. Trans. 41 (2013) 962–967.
[23] H. Saitsu, T. Nishimura, K. Muramatsu, H. Kodera, S. Kumada, K. Sugai, et al., De novo mutations in the autophagy gene WDR45 cause static encephalopathy of childhood with neurodegeneration in adulthood, Nat. Genet. 45 (2013) 445–449 (9e1).
[24] T.B. Haack, P. Hogarth, A. Gregory, H. Prokisch, S.J. Hayflick, BPAN: the only X-linked dominant NBIA disorder, Int. Rev. Neurobiol. 110 (2013) 85–90.
[25] G.L. Carvill, A. Liu, S. Mandelstam, A. Schneider, A. Lacroix, M. Zemel, et al., Severe infantile onset developmental and epileptic encephalopathy caused by mutations in autophagy gene WDR45, Epilepsia. 59 (2018) e5–e13.
[26] H. Najmabadi, H. Hu, M. Garshasbi, T. Zemojtel, S.S. Abedini, W. Chen, et al., Deep sequencing reveals 50 novel genes for recessive cognitive disorders, Nature. 478 (2011) 57–63.
[27] J. Suleiman, D. Allingham-Hawkins, M. Hashem, H.E. Shamseldin, F.S. Alkuraya, A.W. El-Hattab, WDR45B-related intellectual disability, spastic quadriplegia, epilepsy, and cerebral hypoplasia: a consistent neurodevelopmental syndrome, Clin. Genet. 93 (2018) 360–364.
[28] V. Mariella, V.I. Korolchuk, A. Avraham, P. Claudia, F.M. Menzies, J.H. Clarke, et al., PI(5)P regulates autophagosome biogenesis, Mol. Cell 57 (2015) 219–234.
[29] A. Scacioc, C. Schmidt, T. Hofmann, H. Urlaub, K. Kuhnel, A. Perez-Lara, Structure based biophysical characterization of the PROPPIN Atg18 shows Atg18 oligomerization upon membrane binding, Sci. Rep. 7 (2017).
[30] Q.-S. Wang, K.-H. Zhang, Y. Cui, Z.-J. Wang, Q.-Y. Pan, K. Liu, et al., Upgrade of macromolecular crystallography beamline BL17U1 at SSRF, Nucl. Sci. Tech. 29 (2018) 68.
[31] Z. Otwinowski, W. Minor, Processing of x-ray diffraction data collected in oscillation mode, Macromol. Crystallogr. Pt. A 276 (1997) 307–326.
[32] P.D. Adams, P.V. Afonine, G. Bunkoczi, V.B. Chen, I.W. Davis, N. Echols, et al., PHENIX: a comprehensive Python-based system for macromolecular structure solution, Acta Crystallogr. D Biol. Crystallogr. 66 (2010) 213–221.
[33] P. Emsley, K. Cowtan, Coot: model-building tools for molecular graphics, Acta Crystallogr. D Biol. Crystallogr. 60 (2004) 2126–2132.
[34] G.M. Morris, R. Huey, W. Lindstrom, M.F. Sanner, R.K. Belew, D.S. Goodsell, et al., AutoDock4 and AutoDockTools4: automated docking with selective receptor flexibility, J. Comput. Chem. 30 (2009) 2785–2791.
[35] J.C. Phillips, R. Braun, W. Wang, J. Gumbart, E. Tajkhorshid, E. Villa, et al., Scalable molecular dynamics with NAMD, J. Comput. Chem. 26 (2005) 1781–1802.
[36] A.D. M, D. B, M. B, R.L. D, J.D. E, M.J. F, et al., All-atom empirical potential for molecular modeling and dynamics studies of proteins, J. Phys. Chem. B 102 (1998) 3586–3616.
[37] D. Alexander, J. MacKerell, M. Feig, L. Charles, I. Brooks, Improved treatment of the protein backbone in empirical force fields, J. Am. Chem. Soc. 126 (2004) 698–699.
[38] R.B. Best, X. Zhu, J. Shim, P.E.M. Lopes, J. Mittal, M. Feig, et al., Optimization of the additive CHARMM all-atom protein force field targeting improved sampling of the backbone ϕ, ψ and sidechain $\chi 1$ and $\chi 2$ dihedral angles, J. Chem. Theory Comput. 8 (2012) 3257–3273.
[39] W. Humphrey, A. Dalke, K. Schulten, VMD: visual molecular dynamics, J. Mol. Graph. 14 (1996) 33–38.